Biochemistry

pubs.acs.org/biochemistry Article

Heterologous Expression, Purification, and Functional Analysis of the *Plasmodium falciparum* Phosphatidylinositol 4-Kinase III*β*

Anna R. Sternberg and Paul D. Roepe*

Cite This: *Biochemistry* 2020, 59, 2494−2506 Read Online

ACCESS | Metrics & More | Article Recommendations

ABSTRACT: Recently, we heterologously expressed, purified, and analyzed the function of the sole *Plasmodium falciparum* phosphatidylinositol 3-kinase (PI3K), found that the enzyme is a "class III" or "Vps34" PI3K, and found that it is irreversibly inhibited by Fe^{2+}-mediated covalent, nonspecific interactions with the leading antimalarial drug, dihydroartemisinin [Hassett, M. R., et al. (2017) *Biochemistry 56*, 4335−4345]. One of several *P. falciparum* phosphatidylinositol 4-kinases [putative III*β* isoform (PfPI4KIII*β*)] has generated similar interest as a druggable target; however, no validation of the mechanism of action for putative PfPI4K inhibitors has yet been possible due to the lack of purified PfPI4KIII*β*. We therefore codon optimized the *pfpi4kIII*β gene, successfully expressed the protein in yeast, and purified an N-lobe catalytic domain PfPI4KIII*β* protein. Using an enzyme-linked immunosorbent assay strategy previously perfected for analysis of PfPI3K (PfVps34), we measured the apparent initial rate, $K_{m,app}$(ATP), and other enzyme characteristics and found full activity for the construct and that PfPI4KIII*β* activity is most consistent with the class III*β* designation. Because several novel antimalarial drug candidates with different chemical scaffolds have been proposed to target PfPI4KIII*β*, we titrated enzyme inhibition for these candidates versus purified PfPI4KIII*β* and PfVps34. We also analyzed the activity versus purified PfPI4KIII*β* mutants previously expressed in *P. falciparum* selected for resistance to these drugs. Interestingly, we found that a putative PfPI4KIII*β* inhibitor currently in advanced trials (MMV390048; MMV '0048) is a potent inhibitor of both PfVps34 and PfPI4KIII*β*. These data are helpful for further preclinical optimization of an exciting new class of *P. falciparum* PI kinase inhibitor ("PfPIKi") antimalarial drugs.

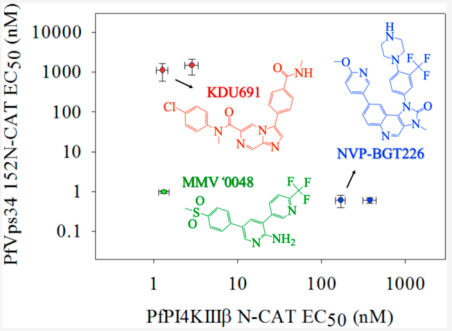

Plasmodium falciparum malaria infects hundreds of millions and kills approximately half a million annually. Historically, the most effective antimalarial control has been the use of antimalarial drugs, including quinoline-based drugs such as chloroquine (CQ) and antifolate compounds [e.g., sulfadoxine/pyrimethamine (SP)]. However, widespread resistance is now found versus both classes; thus, currently, the only drug class that is effective versus all malaria worldwide consists of the artemisinin drugs [artemisinin (ART), artemether (ATM), artesunate (ATS), and dihydroartemisinin (DHA)]. Synthetic ART-based drugs that incorporate or mimic a pharmacologically relevant ART endoperoxide bridge (e.g., OZ277, OZ439, and E209) are currently in development.

Typically, ART drugs are administered in combination with a longer-lasting "partner" drug. Common examples of such "ART combination therapies" (ACTs) are DHA with piperaquine (DHA/PPQ), ATM with lumefantrine (ATM/LF), and ATS with mefloquine (ATS/MQ). Troublingly, however, what may be a precursor to formal ACT resistance, called the "delayed clearance phenotype" (DCP), has emerged in southeast Asia.[1] Recent studies also show an alarming spread of resistance to both drugs within at least one common ACT.[2,3] With a few exceptions, DCP *P. falciparum* parasites do not typically show IC_{50} or LD_{50} shifts versus ART-based drugs in standard drug susceptibility tests; however, in the clinic, DCP patients treated with ACTs show longer parasite clearance rates.[4−6] In the laboratory, DCP parasites are typically characterized by the "ring stage assay" (RSA).[7]

Next-generation ACTs incorporating new partner drugs with novel mechanisms of action (MOA) are desperately needed. Recent high-throughput screening efforts have identified *P. falciparum* class III phosphatidylinositol 3-kinase (PfPI3KIII) and type III*β* phosphatidylinositol 4-kinase (PfPI4KIII*β*) inhibitors as very potent antimalarial drugs, with strong synergy found for artemisinin−PI3K inhibitor drug pairs.[8−12] Previous studies suggest that both PfPI3KIII and PfPI4KIII*β* are essential proteins.[10,13−15] Taken together, these data suggest PfPI3KIII and PfPI4KIII*β* inhibitors ("PfPIKi") are highly attractive candidates for the development of next-generation ACT partner drugs. Accordingly, to test MOA and

Received: March 31, 2020
Revised: June 12, 2020
Published: June 16, 2020

https://dx.doi.org/10.1021/acs.biochem.0c00259
Biochemistry 2020, 59, 2494−2506

other concepts, we recently heterologously expressed, purified, and analyzed drug inhibition for the sole *P. falciparum* PI3K[16] (PfPI3KIII) and have now followed a similar approach for the analysis of PfPI4KIIIβ.

In 2008 and 2013, two new antimalarial drug chemical classes (imidazopyrazine and quinoxaline) were discovered by screening the Novartis Research Foundation Genomics Institute chemical library.[8,10] The imidazopyrazines in particular show considerable promise due to their multistage potency against the parasite, which might be explained by their targeting of an essential protein with relatively consistent expression and activity across life cycle stages.[13] Analysis of imidazopyrazine resistant parasite clones derived by exposure to increasing drug pressure suggested that their MOA is, at least in part, through inhibition of PfPI4K type IIIβ (PF3D7_0509800).[10] Although some measurements versus a *Plasmodium vivax* PI4KIIIβ orthologue were taken to test this idea, no direct measurements versus PfPI4KIIIβ were possible at the time. Several differences exist for the orthologues, including within the conserved catalytic domain. These may affect drug binding and inhibition and the measurement of drug potency versus mutant enzymes. For example, the reduced drug potency observed for *P. falciparum* parasites expressing H1484Y mutant PfPI4KIIIβ was not recapitulated when analyzing H1484Y mutant PvPI4KIIIβ.[10] This suggests that even subtle sequence differences between the two enzymes might result in species-specific activities, which would complicate analysis of the PfPI4KIIIβ enzyme and putative inhibitors.

In 2017, PfPI4KIIIβ was implicated as the target of another novel multistage potent drug candidate, a 2-aminopyridine now known as MMV390048 ("MMV '0048").[12] Genomes of three laboratory-derived MMV '0048 resistant clones were sequenced and, similar to imidazopyrazine resistant clones, were found to have nonsynonymous single-nucleotide polymorphisms (SNPs) within *pfpi4kIIIβ*. While mutations in other genes were also identified, *pfpi4kIIIβ* was the only gene harboring nonsynonymous SNPs in all three sequenced clones.[12]

Interestingly, genetically engineered parasite strains carrying the PI4KIIIβ S1320L or H1484Y mutation showed some resistance to both imidazopyrazines and MMV '0048, suggesting some degree of mutual or overlapping MOA for these two drug classes.[10,12] Affinity capture experiments with the MMV '0048-supplemented parasite lysate further suggested PfPI4KIIIβ as a possible target for MMV '0048.[12]

As mentioned above, previously we successfully heterologously expressed, purified, and characterized the sole *P. falciparum* PI3K. ELISA-based activity measurements clearly showed this PIK to be a class III PI3K (thus now renamed "PfVps34") and along with previous work[11,17] further defined the enzyme as an attractive, novel target for next-generation candidate ACT partner drugs. Due to the high AT content of most *P. falciparum* genes, it is typically quite difficult to express large proteins in heterologous systems, but yeast-based methods used for PfVps34 and other *P. falciparum* proteins[18,19] have been successful in our hands. Following the same approach, we have codon optimized the *pfpi4kIIIβ* gene for heterologous expression in yeast, purified the protein to homogeneity, and adapted a recently validated quantitative assay for measuring the production of PIP from PI[20] to characterize enzyme activity and to quantify inhibition by various drugs. Surprisingly, one leading candidate PfPI4KIIIβ inhibitor is found to be a potent dual kinase inhibitor.

MATERIALS AND METHODS

Materials. Difco yeast nitrogen base extract without amino acids (YNB w/o a.a.) was purchased from BD (Sparks, MD). HIS-Select Nickel affinity gel, anti-mouse IgG-HRP, anti-mouse IgM-HRP, and EDTA-free protease inhibitor cocktail (PIC) were purchased from Sigma (St. Louis, MO). AcTEV protease and anti-V5-HRP were purchased from Invitrogen (Carlsbad, CA). Spectra/Por dialysis tubing was purchased from Spectrum Laboratories, Inc. (Rancho Dominguez, CA). Urea and Amicon Ultra-4 Centrifugal Filter Units were purchased from Millipore (Burlington, MA). Amersham Protran Premium 0.2 μM NC Nitrocellulose and Amersham ECL Plus Western blotting detection reagents were purchased from GE Healthcare (Piscataway, NJ). All phosphoinositide lipids and lipid antibodies were purchased from Echelon Biosciences (Salt Lake City, UT). Streptavidin-coated plates and a 3,3′,5,5′-tetramethylbenzidine (TMB) substrate solution were purchased from ThermoFisher Scientific (Waltham, MA). All other reagents were reagent grade or better and were purchased from Sigma.

PfPI4KIIIβ Construct Design. The sequence for *P. falciparum* gene PF3D7_0509800 (*pfpi4kIIIβ*) was acquired from PlasmoDB (plasmodb.org), and EuGene gene optimization software (UA.PT Bioinformatics) was used to design theoretically optimized genes using a *Saccharomyces cerevisiae* yeast codon usage table (previously described in ref 18). Similar to our previously published approach for PfPI3KIII (PfVps34),[16] PfPI4KIIIβ "N-CAT" and "CAT" constructs encoding partial N-lobe and full catalytic domains and the full catalytic domain alone, respectively [encoding residues 1261−1559 and 1357−1559, respectively (see Results and Discussion)] were further designed. One codon-optimized gene encoding PfPI4KIIIβ "N-CAT" was synthesized by GenScript (Piscataway, NJ), and the PfPI4KIIIβ "CAT" construct was derived from N-CAT by polymerase chain reaction. Mutant N-CAT constructs were created via site-directed mutagenesis (Agilent, Santa Clara, CA) as previously described[18,19,21] using the following oligonucleotide primers: CAGGAGTTGTTGGCCCTCCAGCTCATCAAGCAG (S1320L), GGTATCATCGAGTTCGTCAACGACACCTGC (Y1356F), and GAGGCCAGAAAGTACTCCGAGGAGATC (H1484Y). All PfPI4KIIIβ gene constructs were fused in tandem to a C-terminal TEV protease recognition site, a hexa-His tag (h), and a V5 epitope (v) for protein purification and visualization. All constructs were expressed in *Pichia pastoris* using the pPicZ methanol-inducible system as described in refs 18 and 19 (see below).

Protein domain assignments were made on the basis of previous domain assignments for the PI4K type IIIβ human orthologue, PI4KB (UniProt Q9UBF8) and were further informed by predicted secondary structures of the native full-length sequence (PredictProtein.org[22]) and comparison to the human PI4KIIIβ crystal structure [Protein Data Bank (PDB) 4d0l[23]]. The PfPI4KIIIβ CAT construct includes all catalytic domain residues as shown by a high degree of homology to the catalytic domains of numerous other eukaryotic PI kinases[23−30] (see Results and Discussion). The N-CAT construct consists of a clear PIK catalytic domain and a C-terminal N-lobe domain as defined previously for eukaryotic PI4K enzymes[10,23−30] and PfVps34.[16]

https://dx.doi.org/10.1021/acs.biochem.0c00259
Biochemistry 2020, 59, 2494−2506

Heterologous Expression in Yeast. PfPI4KIIIβ expression in *P. pastoris* and isolation of yeast membranes were performed as described previously for PfVps34.[16] Briefly, expression was induced by addition of 0.5% methanol [minimal methanol medium (MMM)]. After 24 h in MMM, cultures were harvested at 3000*g* [5 min, room temperature (RT)] and washed three times with harvest buffer [100 mM glucose, 50 mM imidazole, and 5 mM DTT (pH 7.5)], and cell pellets were then resuspended in breaking buffer [100 mM glucose, 250 mM sucrose, 50 mM imidazole, 1 mM $MgCl_2$, 5 mM DTT, and PIC at 1 tablet per 50 mL (pH 7.5)] at 2 mL/g of wet cell weight. Cells were lysed via a French press (Sim-Aminco) at 20000 psi. Unlysed cells and cell debris were removed, and the remaining lysate was centrifuged at 100000*g* to isolate the yeast membrane fraction containing copious PfPI4KIIIβ (see Results and Discussion). Protein was quantified, and membranes were stored at −20 °C (−80 °C for long-term storage) prior to Western blot analysis and PfPI4KIIIβ purification.

Protein Purification. Membranes harboring PfPI4KIIIβ were prewashed with *n*-dodecyl β-D-maltoside (DDM) prior to a chaotropic urea wash. They were resuspended in 0.3% DDM [in 16 mM Na_2HPO_4, 4 mM KH_2PO_4, 500 mM NaCl, and 10 mM BME (pH 7.4)] at a concentration of 2 mg/mL, mixed at 4 °C for 30 min, and then centrifuged at 100000*g* for 1 h. The supernatant was discarded, and the membrane pellet resuspended in extraction buffer ["EB"; 4 M urea, 16 mM Na_2HPO_4, 4 mM KH_2PO_4, 500 mM NaCl, 20 mM BME, and PIC at 1 tablet per 50 mL (pH 7.4)], mixed at 4 °C for 30 min, and centrifuged again at 100000*g* for 1 h. The supernatant was dialyzed overnight at 4 °C versus dialysis buffer [10 mM Tris, 70 mM sucrose, 140 mM KCl, and 2.5 mM BME (pH 7.5)] to remove urea and any remaining DDM.

HIS-Select Nickel affinity gel was equilibrated at 4 °C with wash buffer [16 mM Na_2HPO_4, 4 mM KH_2PO_4, 500 mM NaCl, 20 mM imidazole, and 10 mM BME (pH 7.4)] prior to application of dialyzed DDM/urea extract containing PfPI4KIIIβ. After sample application, the column was washed with 100 mL of wash buffer and His-tagged protein was then eluted with 12 mL of elution buffer [16 mM Na_2HPO_4, 4 mM KH_2PO_4, 500 mM NaCl, 500 mM imidazole, 5 mM BME, and PIC at 1 tablet per 50 mL (pH 7.4)]. The eluate was dialyzed for 23 h at 4 °C versus three changes of 4 L of dialysis buffer to remove imidazole. Dialyzed samples were then incubated overnight at RT with 4 μL of AcTEV protease (10 units/μL) with rotation to remove hexa-His and V5 tags. The sample was then applied to a fresh HIS-Select Nickel affinity column pre-equilibrated with dialysis buffer at 4 °C. PfPI4KIIIβ N-CAT was collected in the column flow-through and spin-concentrated using an Amicon Ultra-4 Centrifugal Filter Unit (Millipore) with a 30 kDa cutoff. Concentrated purified PfPI4KIIIβ was stored in a 10% glycerol solution at −20 °C. Prior to biochemical analysis, the total protein concentration for the purified enzyme was determined by the Bradford assay.

PfVps34 protein "152N-CAT" was purified as described previously.[16]

Lipid Antibody "Dot Blot". Lyophilized lipids were reconstituted in a 1:1 $CHCl_3/CH_3OH$ mixture to prepare 1 mM stock solutions and stored at −80 °C prior to use. Nitrocellulose membranes were equilibrated in doubly distilled (dd) H_2O, while lipid dilutions were prepared in a 2:1:0.8 $CH_3OH/CHCl_3/H_2O$ mixture. Presoaked membranes were placed on Kimwipes on top of foil to remove excess liquid during spotting; 1.5 μL of each PI, PI3P, and PI4P dilution was spotted onto the nitrocellulose. Membranes were allowed to dry for 1 h on foil in the dark at RT. Membranes were blocked with blocking buffer {3% bovine serum albumin (BSA) in TBS-T [25 mM Tris, 130 mM NaCl, 2.7 mM KCl, and 0.1% Tween 20 (pH 7.4)]} for 1 h at RT while being lightly shaken. Blocking buffer was discarded, and membranes were incubated in the primary antibody [1 μg/mL anti-PI3P mouse IgG (Echelon Biosciences) in blocking buffer] overnight at 4 °C while being lightly shaken. Membranes were washed three times with TBS-T and then incubated in the secondary antibody (1.25 μg/mL anti-mouse IgG-HRP in blocking buffer) for 1 h at RT. Membranes were washed three times with TBS-T once again prior to development of HRP using Amersham ECL Plus Western blotting detection reagents. Dot blots were exposed to BLU-C autoradiography film (Stellar Scientific, Baltimore, MD) and developed using a Konica SRX-101A medical film processor (Konica Corp., Tokyo, Japan).

PI4K ELISA. Ninety-six-well streptavidin-coated plates (ThermoFisher Scientific) were washed three times with TBS-T prior to being coated with biotinylated PI4P (b-PI4P; 10 pmol per well) for 2 h while being lightly shaken.[16] Plates were covered with SealPlate (Sigma) to prevent potential solvent loss due to evaporation during the 2 h incubation; 50 ng of the purified enzyme (plus 10× drug stock) was equilibrated to 37 °C for 30 min prior to the enzyme assay, which was initiated by the addition of reaction buffer [10 mM Tris, 150 mM NaCl, and 10 mM $MgCl_2$ (pH 7.4)] with 50 μM ATP and 16 μM PI. Final reaction volumes were 25 μL with either 84 nM PfPI4KIIIβ CAT, 57 nM PfPI4KIIIβ N-CAT, or 48 nM PfVps34 152N-CAT and <0.1% DMSO in each case. The reaction time varied (see Results and Discussion) but was typically 15 min. Reactions were stopped by the addition of 100 mM EDTA to a final concentration of 17 mM. Reaction mixtures were diluted with detection buffer [10 mM Tris, 150 mM NaCl, 7.5 mM EDTA, and 1 mM DTT (pH 7.4)] prior to plating. For the generation of standard curves, PI4P was dissolved in the reaction−detection buffer mixture to mimic the diluted enzyme reaction mixture. b-PI4P-equilibrated plates were washed three times with TBS-T, and PI4P standards and enzyme reaction mixtures were then plated in at least duplicate and incubated for 1 h with 0.5 μg/mL anti-PIP mouse IgG or anti-PI4P mouse IgM (see Results and Discussion). Plates were washed four times with TBS-T. Wells were then incubated with anti-mouse IgG-HRP or anti-mouse IgM-HRP (final concentration of 1.25 μg/mL) for 30 min while being lightly shaken and washed four times with TBS-T, and the HRP signal was developed by incubating wells with 100 μL of a 3,3′,5,5′-tetramethylbenzidine (TMB) substrate solution for 30 min with light shaking in the dark. Development was quenched by the addition of 100 μL of 500 mM sulfuric acid, and A_{450} was measured with an EnSpire Multimode plate reader (PerkinElmer, Waltham, MA). As described previously,[16,20] the PI4P signal is inversely proportional to [PI4P] within individual wells (see Results and Discussion). The percent activity was relative to the activity measured in the absence of drug (100% activity), and inhibition curves were fitted using SigmaPlot software.

Western Blotting. Western blotting was performed with anti-V5-HRP as previously described.[21]

Homology Modeling. The SWISS-MODEL web-based protein structure homology modeling tool (Swiss Institute of Bioinformatics[31]) was used to build a PfPI4KIIIβ N-CAT

https://dx.doi.org/10.1021/acs.biochem.0c00259
Biochemistry 2020, 59, 2494−2506

homology model using the human PI4KIIIβ crystal structure (PI4KB, PDB entry 4d0l[23]) as a template. The SWISS-MODEL server's ProMod3 comparative modeling engine utilizes amino acid alignment between target and template proteins to guide building of a target protein homology model based on the template protein's structure. The resulting PfPI4KIIIβ N-CAT homology model had a global model quality estimation (GMQE) score of 0.72/1.0, indicating a high level of expected model accuracy for this particular alignment (43.8% identity), template (SMTL ID 4d0l.3.A/PDB entry 4D0L chain E), and model coverage of the target protein sequence (88% coverage).

RESULTS AND DISCUSSION

Gene Optimization and Expression. Recent homology analysis has suggested that the *P. falciparum* gene PF3D7_0509800 encodes a phosphatidylinositol 4-kinase type IIIβ.[10,12,24,32] Sequence alignment shows the most homology with HsPI4KB (UniProt Q9UBF8), which is a type IIIβ enzyme. On the basis of catalytic loop sequence alignment, PF3D7_0509800 is identified as a PI4K (Figure 1).

PfPI4KIIIß	1411	KDRHNGNLLLDSDGHLIHIDYGFMLT	1436
HsPI4KIIIß	670	KDRHNGNILLDAEGHIIHIDFGFILS	695
ScPIK1	917	KDRHNGNIMIDNEGHVSHIDFGFMLS	942
HsVps34	742	GDRHLDNLLLTKTGKLFHIDFGYILG	767
ScVps34	730	GDRHLDNLLVTPDGHFFHADFGYILG	755
PfVps34	1989	GDRHLDNLMVTKDGRFFHIDFGYIFG	2014

Figure 1. Alignment of catalytic and activation loop residues in PfPI4KIIIβ. Identity with respect to PfPI4KIIIβ is underlined; conserved residues are colored red. PfPI4KIIIβ residues that are identical (highlighted) and conserved (red) among class III PI3Ks and type III PI4Ks are indicated.

The catalytic loop interacts with the DFG motif of the activation loop.[33] The location and orientation of charged residues surrounding the conserved DRH motif likely aid in phosphate transfer to the correct inositol hydroxyl. The catalytic loop also harbors a highly conserved KDRHNGN motif,[34] which is rearranged for PI3K enzymes.[35] Type III PI4Ks contain a catalytic domain consensus sequence distinct from that of type II PI4Ks.[36]

Along with strong homology to HsPI4KIIIβ (Figure 1), structural analysis of HsPI4KIIIβ (PDB entry 4d0l[23]), previous domain assignments,[10,23−30] and sequence-based predictions of secondary structure informed our assignments of the PfPI4KIIIβ helical, N-lobe, and catalytic domain regions (Figure 2A). As with many other *P. falciparum* proteins, the *Pf* protein sequence is approximately twice the size of its human orthologue due to long inserted stretches of low-complexity regions throughout the protein [N,D repeats (see ref 16)]. Regardless, a high degree of sequence homology between the *Hs* and *Pf* C-termini via EMBL EMBOSS Needle global pairwise alignment clearly identifies the PfPI4KIIIβ C-terminal half as containing the proximal N-lobe and catalytic domains necessary for full activity (Figure 2). Previously, Burke et al. defined Pf-Y1356 as being equivalent to the *Hs* hinge residue P597, thereby assigning Pf-V1357 as the first residue in the catalytic domain for the *Pf* enzyme.[23] NCBI BLAST search results for the *Hs* helical domain (residues 128−243[23,30]) versus the *Pf* sequence combined with predicted *Pf* secondary structure define the PfPI4KIIIβ helical domain as residues 371−485 (Figure 2). Predicted *Pf* secondary structure closely resembling *Hs* secondary structure suggested the *Pf*-equivalent N-terminal N-lobe region is located near residues 712−842. EMBOSS Needle alignment showed the closest alignment between *Hs* N-terminal N-lobe residues 321−405 and *Pf* residues 728−843 (not shown).

Previously, McNamara et al. annotated the PfPI4KIIIβ catalytic domain as residues 1261−1559,[10] which is in general agreement with our analysis. To account for any small discrepancies between our domain assignments for the PfPI4KIIIβ catalytic domain, we synthesized and heterologously expressed an "N-CAT" protein construct to ensure inclusion of the entire catalytic domain as defined by McNamara et al. (Figure 2B), which according to our assignments also includes the C-terminal N-lobe and hinge regions. Previously, we found that a similar PfVps34 construct retained full activity.[16] In agreement with this, full sequence alignment of PfPI4KIIIβ versus PfVps34 reveals the highest degree of homology for PI4KIIIβ catalytic domain residues 1282−1559 (not shown). Also consistent with this analysis, previous work found that heterologous expression of PfPI4KIIIβ constructs lacking N-terminal residues 116−1220

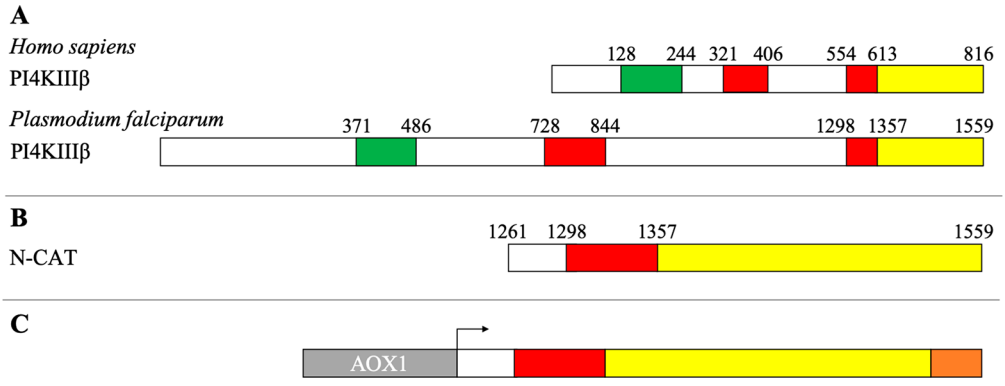

Figure 2. Domain assignments for PfPI4KIIIβ based on sequence and secondary structure alignments vs *Homo sapiens* PI4KIIIβ and its previously assigned domains.[10,23−30] (A) Predicted helical (green), N-lobe (red), and catalytic (yellow) domains. HsPI4KIIIβ has a large insertion in the N-lobe,[23] which appears to be present also in the PfPI4KIIIβ but is larger for the *Pf* enzyme. (B) The N-CAT protein expressed in this study contains the entirety of the PfPI4KIIIβ catalytic domain, as well as the C-terminal portion of the N-lobe. (C) Schematic of the PfPI4KIIIβ N-CAT protein expressed in *P. pastoris* under AOX1 promoter induction (gray) with the TEV protease recognition site, hexa-His tag, and V5 epitope fused in frame at the C-terminus (orange).

https://dx.doi.org/10.1021/acs.biochem.0c00259
Biochemistry 2020, 59, 2494−2506

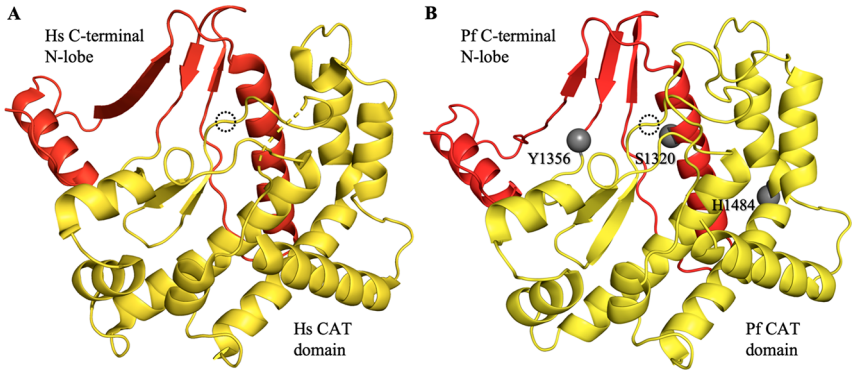

Figure 3. Homology model of PfPI4KIIIβ N-CAT (B) based on sequence alignment with the known HsPI4KIIIβ structure (A; PDB entry 4d0l[23]). Putative N-lobe and catalytic domains are colored red and yellow, respectively. Locations of key PfPI4KIIIβ residues [gray spheres (see Results and Discussion)] (B) are based on orthologous residues for HsPI4KIIIβ (A). The homologous activation loop is circled with a dotted line (A and B).

was capable of fully complementing the impaired growth phenotype of a temperature-sensitive mutant yeast strain ($\Delta pik1^{ts}$) defective in the expression of the yeast PI4K orthologue, PIK1.[24]

To further test domain assignments, local sequence alignment of PfPI4KIIIβ N-CAT with a human PI4KIIIβ crystal structure[23] facilitated homology modeling (Figure 3). Alignment of PfPI4KIIIβ N-CAT versus the *Hs* enzyme revealed 43% identity and 65.9% homology between the two sequences. Homologous domain residues in the HsPI4KIIIβ crystal structure corresponding to those contained in PfPI4KIIIβ N-CAT are colored red (N-lobe region) and yellow (catalytic domain) in Figure 3A. The validity of this model is supported by excellent homology (62.3%) between the CAT domains of both enzymes and an even higher level of homology (74.6%) for the C-terminal N-lobe domain sequences (red, Figure 3). The proposed structure of the PfPI4KIIIβ N-CAT elucidated by SWISS-MODEL (see Materials and Methods) is shown in Figure 3B.

Purification and *In Vitro* Characterization of PfPI4-KIIIβ. PfPI4KIIIβ was expressed in yeast (Figure 4), and protein was purified as described in Materials and Methods. Briefly, all constructs encoded a C-terminal tag comprised of a TEV protease recognition site, a hexa-His tag, and a V5 epitope (Figure 2C) that was used for tandem positive–negative His purification via affinity chromatography (Figure 5). Protein recovery at each step of the purification except the last was visualized via an anti-V5 Western blot (Figure 5A), and the final, concentrated purified protein lacking all C-terminal tags post-TEV cleavage was visualized via silver stain (Figure 5B). Assuming a lower limit of 0.05–0.1% of total yeast membrane protein for PfPI4KIIIβ similar to other proteins,[18,19] we estimate an expression yield of 0.5–1 μg of recombinant protein per milligram of total membrane protein and >1000-fold purification for PfPI4KIIIβ.

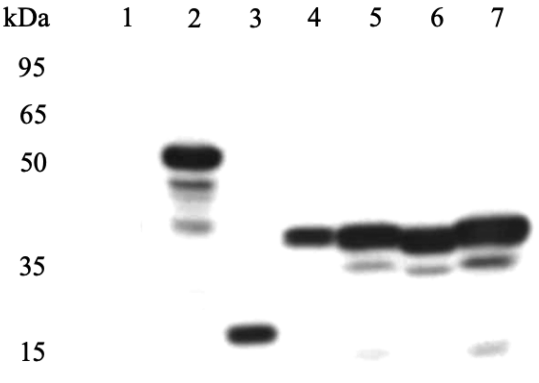

Figure 4. Heterologous expression of the various *Pf* PIK proteins and mutants discussed in this paper. Lane 1 contained the yeast membranes from yeast harboring the empty expression vector (EV). The masses of PfVps34 152N-CAT (lane 2), PfPI4KIIIβ CAT (lane 3), and PfPI4KIIIβ N-CAT (lanes 4–7) proteins are 52.9, 26.9, and 38.2 kDa, respectively. PfPI4KIIIβ N-CAT S1320L (lane 5), N-CAT Y1356F (lane 6), and N-CAT H1484Y (lane 7) mutants are expressed at levels similar to that of the wild type (lane 4).

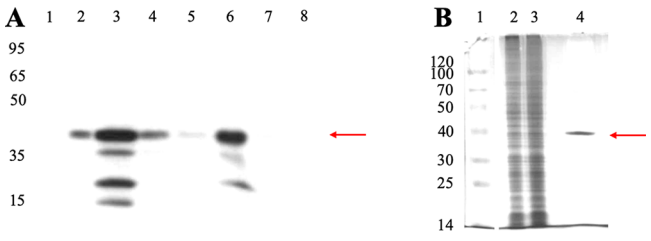

Figure 5. Purification of PfPI4KIIIβ. (A) An anti-V5 Western blot was used to monitor recovery during purification: lane 1, yeast membranes from yeast expressing the empty expression vector (EV); lane 2, 5 μg of membranes from yeast expressing PfPI4KIIIβ N-CAT; lane 3, ~45 μg of urea-solubilized PfPI4KIIIβ; lane 4, Ni^{2+} column flow-through; lane 5, column wash; lane 6, column eluate; lane 7, same as lane 6 but post-TEV treatment; lane 8, same as lane 7 but flow-through from post-TEV second Ni^{2+} column (see Materials and Methods). (B) Concentrated purified PfPI4KIIIβ [lane 4, recovered material as in lane 8 of panel A (see Materials and Methods)] was visualized via silver staining vs protein standards (lane 1), as well as equivalent yeast membranes isolated from strains harboring either the empty vector (lane 2) or the PfPI4KIIIβ expression vector (lane 3).

To analyze purified PfPI4KIIIβ kinase activity, we adapted an ELISA, which we previously validated[20] for the quantitative measurement of PI3K activity, for quantification of PI4P (Figure 6A). We found that an available anti-PI4P mouse IgM (Echelon Biosciences) was not sufficiently sensitive to distinguish micromolar amounts of PI4P from other PI lipids (data not shown). However, fortuitously, we found that an available anti-PIP IgG (see Materials and Methods) with good reactivity versus PI3P[16,20] was cross-reactive with PI4P in a concentration-dependent manner (Figure 6B). The antibody shows a low affinity for PI, with a much higher affinity for the PI4P lipid and even higher for PI3P (Figure 6B). Thus, under

https://dx.doi.org/10.1021/acs.biochem.0c00259
Biochemistry 2020, 59, 2494–2506

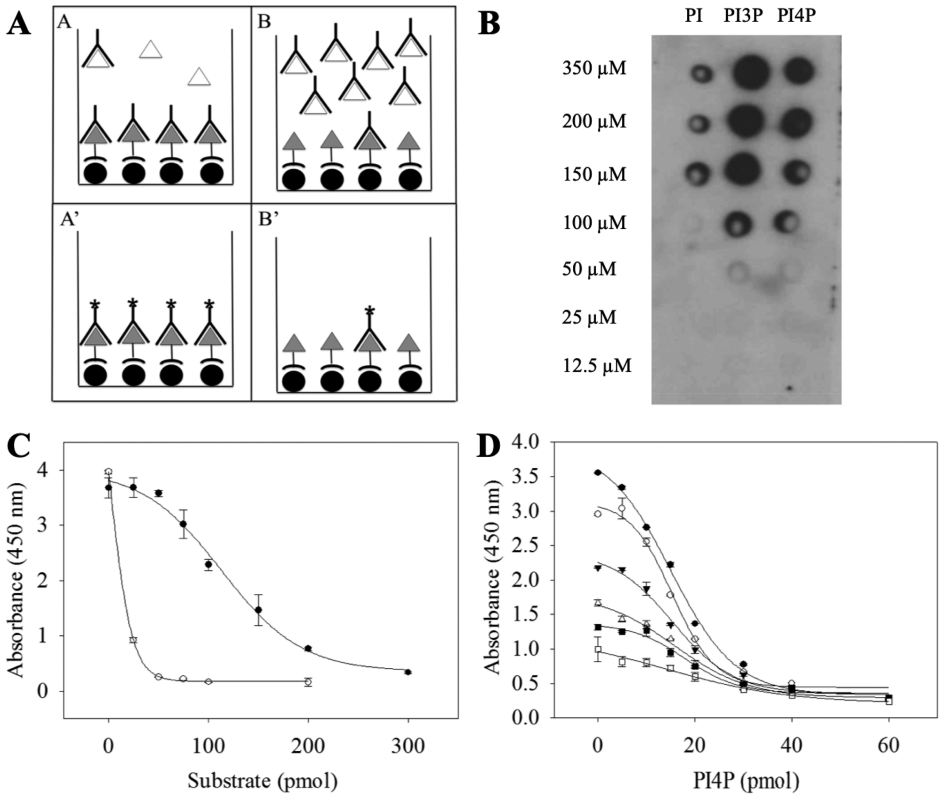

Figure 6. ELISA[20] for PI4P detection and quantification. (A) Schematic of the assay format via which the moles of PIP product formed per unit time is quantified. Biotinylated PI4P (gray triangles) is bound to streptavidin (black circles)-coated wells. Varying amounts of exogenous PI4P (white triangles) is added to the wells as a product of enzyme activity or standard curve titration (subpanels A and B). Exogenous PI4P competes with bound PI4P for a PIP antibody (black Y). Addition of a secondary antibody (*) allows for chemiluminescent detection of bound IgG (subpanels A′ and B′). Increasing amounts of exogenous PI4P decrease the amount of bound IgG (subpanel A vs subpanel B), resulting in a decrease in the intensity of the signal (subpanel A′ vs subpanel B′). (B) A lipid dot blot (see Materials and Methods) titrating PI, PI3P, and PI4P vs Echelon anti-PIP mouse IgG shows the cross-reactivity of the antibody. (C) Titration of PI (●) and PI4P (○) to determine the anti-PIP antibody specificity in the ELISA format. (D) Increasing amounts of PI added in the presence of PI4P dampen the PI4P-dependent signal. A constant amount of PI ranging from 0 pmol (top, ●) to 150 pmol (bottom, □) was added to each PI4P titration (x axis).

standard assay conditions, exogenously added PI and PI4P were titrated to quantify specificity for PI4P over PI in our ELISA format (Figure 6C). When plates were coated with 10 pmol of biotinylated PI4P (b-PI4P) per well, the antibody signal was lost as increasing amounts of exogenous PI4P (○) were added, with complete loss of signal by 50 pmol of PI4P. Upon titration of the PI concentration (●), there is minimal loss of signal up to 50 pmol of PI, with a decrease in the intensity of the signal then seen with >50 pmol of PI (see also ref 20). Direct PI versus PI4P competition for the antibody is shown in Figure 6D, in which wells were coated with 10 pmol of b-PI4P and exogenous PI4P was titrated in the presence of an increasing PI concentration. As expected, a higher PI concentration resulted in a progressive loss of signal to noise as PI competes for the antibody at these concentrations (see ref 20). To employ a substrate concentration as close to type III PI4K K_m(PI) as possible without sacrificing the signal to noise, we fixed the PI concentration at 100 pmol per well (reaction concentration of 16 μM), which is close to estimates of K_m(PI) for human PI3Ks and mammalian type II PI4Ks.[37−40]

PI4KIIIβ enzymes produce only PI4P from only PI.[38] The production of PI4P from PI was measured under standard assay conditions as described in Materials and Methods. PfPI4KIIIβ N-CAT is fully active with an apparent initial rate of 72.5 nmol min^{-1} mg^{-1} (Figure 7A and Table 1), well within the range of values previously measured for various human PI4KIIIβ preparations from multiple laboratories [27−89 nmol min^{-1} mg^{-1},[47−50] (Table 1)]. The PfPI4KIIIβ CAT construct [comprising only the catalytic domain (see above)] shows approximately 50% activity versus PfPI4KIIIβ N-CAT (Figure 7C), similar to previous results for PfVps34,[16] suggesting that the N-lobe and complete hinge region are not obligate for, but do enhance, kinase activity. Under standard assay conditions, we varied the ATP concentration and measured an apparent K_m(ATP) of 79 μM for PfPI4KIIIβ N-CAT (Figure 7B and Table 1), which is slightly lower compared to some published values for human type III PI4K[52] but similar to other K_m(ATP) values for the human type III α and β as measured in "ADP-Glo" assay format (70 and 90 μM, respectively).[51] In comparison, human type II PI4K K_m(ATP) values range from 100 to 120 μM[44] and the enzymes show initial rates of >150 nmol min^{-1} mg^{-1}.[41−43] Ca^{2+} sensitivity at high (10 mM) versus low (0.5 mM) Mg^{2+} concentrations changes dramatically for human type II PI4K (by 2 orders of magnitude),[44] but to the best of our knowledge, such large changes have not previously been noted for type III enzymes. PfPI4KIIIβ shows relatively small changes in Ca^{2+} sensitivity (Table 1). Taken together then, although the measured apparent K_m(ATP) is somewhat ambiguous, overall these data are most consistent with a IIIβ designation for PfPI4KIIIβ N-CAT.

These findings are in agreement with previous sequence analyses and growth complementation in a PIK1 loss of

https://dx.doi.org/10.1021/acs.biochem.0c00259
Biochemistry 2020, 59, 2494−2506

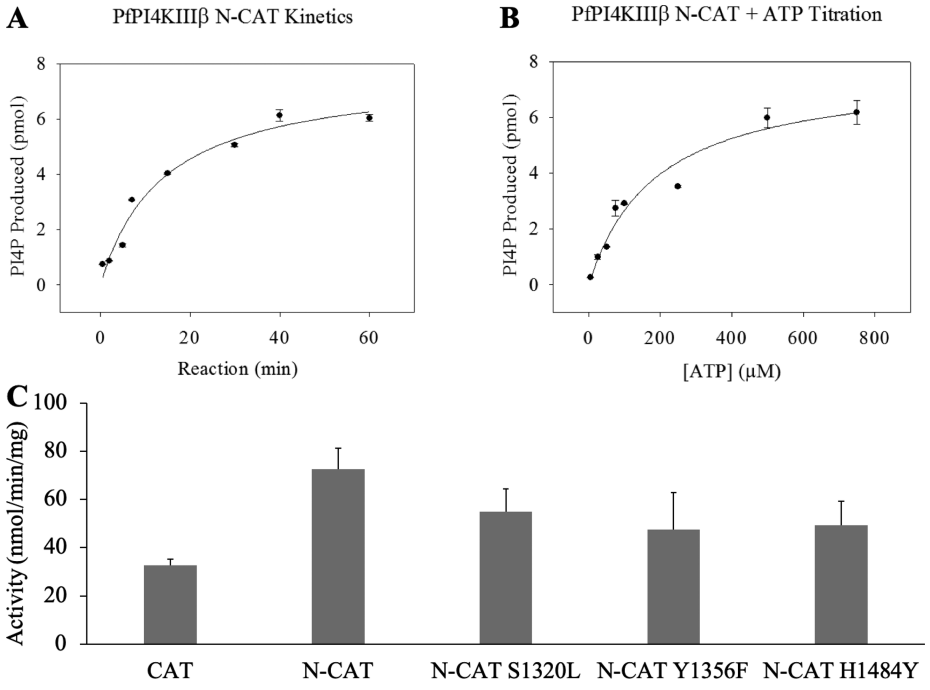

Figure 7. Biochemical characterization of PfPI4KIIIβ. (A) Raw data showing the product produced vs time under standard assay conditions for the PfPI4KIIIβ N-CAT protein (see the text). (B) The ATP concentration was titrated to determine an apparent K_m(ATP) of 79 μM for the PfPI4KIIIβ N-CAT protein. (C) Comparison of apparent initial rate activities for the wild type CAT and N-CAT vs mutant enzymes.

Table 1. Summary of Previously Published PI4K Enzyme Characteristics versus Those Measured for PfPI4KIIIβ and PfVps34[a]

	initial rate (nmol min^{-1} mg^{-1})	K_m(ATP) (μM)	Ca^{2+} EC_{50}
type II PI4K	155.1−991.5 (*Hs*)[41−43]	100−120 (*Hs*)[44]	3 μM (at 0.5 mM Mg^{2+}), 200 μM (at 10 mM Mg^{2+}) (*Hs*)[44] 300 μM (at 10 mM Mg^{2+}), 2 μM (at 20 mM Mg^{2+}) (bovine)[45,46]
type III PI4K	27−88.6 (*Hs*)[47−50]	70−209 (*Hs*)[51,52]	>100 μM (at 20 mM Mg^{2+}) (bovine)[46]
PfPI4KIIIβ N-CAT	72.5 ± 8.80	79.1 ± 7.61	56.2 μM (at 0.5 mM Mg^{2+}), 73.6 μM (at 10 mM Mg^{2+})
PfVps34 1S2N-CAT	123[16]	63.7[16]	58.5 μM (at 10 mM Mn^{2+})

[a]Measurements for PfVps34 and PfPI4KIIIβ (at least two independent experiments each performed in triplicate) are compared to previously published data for mammalian PI4Ks as cited within the table.

function yeast model ($\Delta pik1^{ts}$).[10,12,24,32] PIK1 is a PI4K; accordingly, attempts to complement PIK1 loss of function in yeast by Vps34 (and other PI3P-producing kinases) were unsuccessful.[53]

Analysis of PfPI4KIIIβ Inhibitors. Several drug resistance-associated SNPs (S1320L, Y1356F, and H1484Y) that originate upon selection of *P. falciparum* with two putative PfPI4KIIIβ-targeting drugs (BQR695 and KAI407) are located within our N-CAT construct[10,12] (Figure 3B). We expressed and purified these mutant PfPI4KIIIβ proteins (Figure 4) and found that in the absence of a drug, all mutants showed a decreased apparent initial rate relative to that of wild type (WT) PfPI4KIIIβ (Figure 7C).

A growing body of work suggests that PfPI4KIIIβ is the target for several novel classes of potent, antimalarial drugs.[10,12,54−57] For example, the growth of live parasites in the presence of imidazopyrazine, quinoxaline, or 2-amino-pyridine lead compounds selects for either PfPI4KIIIβ amino acid substitutions or *pfpi4kIIIβ* gene amplification suggestive of a common MOA.[10,12] However, although inhibition activity for some drugs has been measured versus a *P. vivax* orthologous enzyme,[10,12,55,56] no direct measurements of inhibition versus PfPI4KIIIβ have been possible until now. We find that representative members of these three new drug classes (the imidazopyrazine KDU691, the quinoxaline BQR695, and the 2-aminopyridine MMV '0048) do indeed inhibit purified PfPI4KIIIβ *in vitro* with potency that is similar (but not identical) to that seen previously versus the PvPI4KIIIβ orthologue (Figure 8 and Table 2).[10,12]

Although more work with additional compounds from these classes clearly remains to be done, we find that the MMV '0048 and KDU691 compounds inhibit PfPI4KIIIβ with a slightly higher potency (both at ∼1.3 nM) versus the quinoxaline BQR695 (∼2.9 nM) (Table 2), similar to previous measurements versus PvPI4KIIIβ (3.4, 1.5, and 3.5 nM vs MMV '0048, KDU691, and BQR695, respectively) with the exception that MMV '0048 is significantly more potent versus the *Pf* enzyme. Not surprisingly, we find that the previously described PI3K-specific inhibitor NVP-BGT226,[20,60] which is quite potent versus previously purified PfVps34 (0.6 nM),[16] is conspicuously less potent versus PfPI4KIIIβ (169 nM).

As expected, both KDU691 and BQR695, believed to target PfPI4KIIIβ, are more potent inhibitors of this enzyme versus PfVps34 [1.26 and 2.85 nM vs 1.11 and 1.48 μM, respectively (Figure 8 and Table 2)]. However, surprisingly, we find that the 2-aminopyridine MMV '0048 is approximately equally potent versus both enzymes (1.32 and 0.98 nM, respectively), which suggests that its increased antimalarial potency relative

https://dx.doi.org/10.1021/acs.biochem.0c00259
Biochemistry 2020, 59, 2494−2506

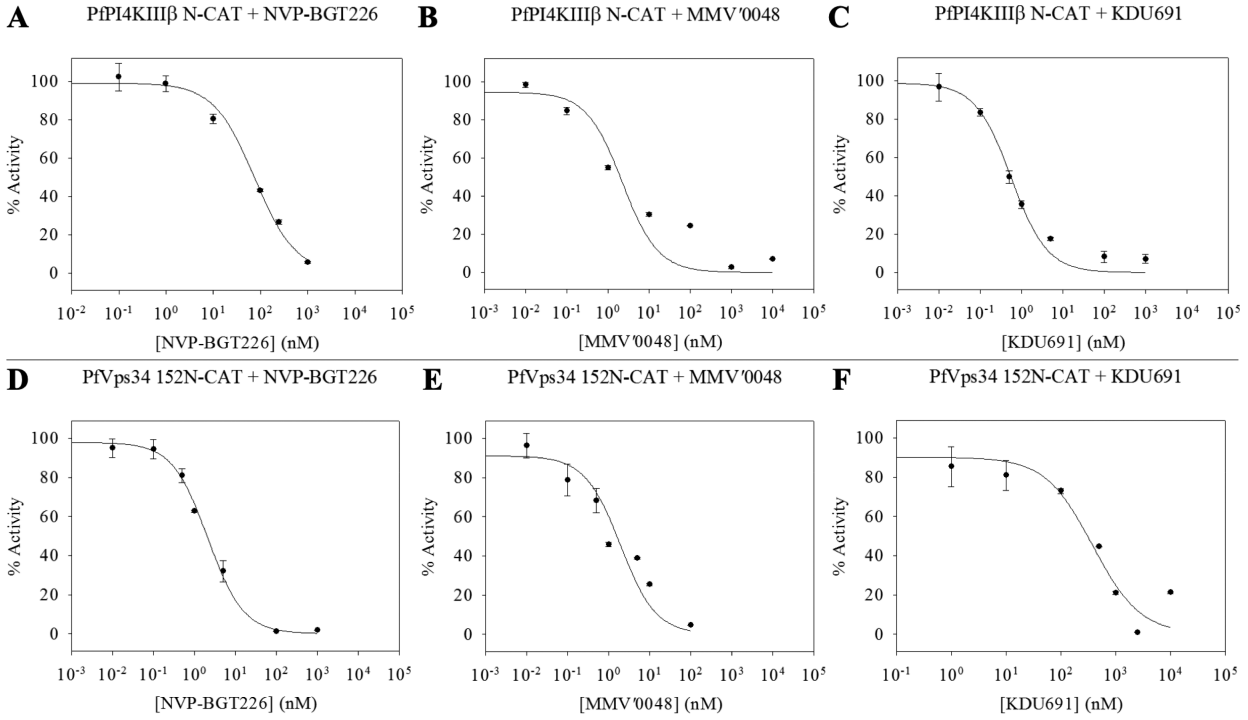

Figure 8. Inhibition of *Pf* PIK enzymes (PfPI4KIIIβ, top panels; PfPI3KIII, bottom panels) by PI3K (NVP-BGT226, left)- and PI4K (MMV '0048 and KDU691, middle and right, respectively)-targeting drugs. Inhibition was visualized as the percent of enzyme activity obtained in the absence of a drug. (A−C) Representative data for three drugs vs purified PfPI4KIIIβ. (D−F) Representative data for the same drugs vs purified PfVps34 (PfPI3KIII).

Table 2. Summary of PI3K- and PI4K-Targeting Drug EC_{50} Values versus Purified *Plasmodium* PIK Enzymes[a]

	PfVps34 152N-CAT		PfPI4KIIIβ N-CAT		
	average	SEM	average (nM)	SEM	previously published EC_{50}
NVP-BGT226	0.6 nM[58]	0.2	169	21.8	7.03 nM (HsVps34)[20]
Torin2	0.6 nM[58]	0.1	379	68.1	18.3 nM (HsPI4KIIIβ)[59]
MMV '0048	0.98 nM	0.08	1.32	0.18	3.4 nM (PvPI4KIIIβ)[12]
KDU691	1.11 μM	0.52	1.26	0.20	1.5 nM (PvPI4KIIIβ)[10]
BQR695	1.48 μM	0.65	2.85	0.53	3.5 nM (PvPI4KIIIβ)[10]

[a]EC_{50} is the concentration of drug at which 50% of purified PfPIK activity is inhibited. EC_{50} values vs PfVps34 and PfPI4KIIIβ (at least three independent experiments, each performed in triplicate) are compared to available previously published data vs HsVps34, HsPI4KIIIβ, or PvPI4KIIIβ.

to the other compounds may be due to previously unrecognized dual kinase inhibitor activity. Further exploring these pharmacophores and others to define chemical features that distinguish dual kinase versus single kinase inhibition should prove to be interesting.

We next explored drug inhibition versus PfPI4KIIIβ mutant proteins (S1302L, Y1356F, and H1484Y) that were previously found to be expressed in parasite strains selected for resistance versus either imidazopyrazine or quinoxaline compounds.[10] Imidazopyrazine-selected parasites expressing the H1484Y PI4KIIIβ mutant isoform were found to be ∼3-fold less sensitive to several structurally similar imidazopyrazines (KAI407, KDU691, and KAI715), and quinoxaline-selected strains expressing S1320L or Y1356F PI4KIIIβ were previously found to be ∼4- or 20-fold resistant to the quinoxaline BQR695, respectively,[10] with the caveat that the Y1356F-expressing strain also showed PfPI4KIIIβ gene amplification. Genetically engineered parasites expressing the H1484Y, S1320L, and Y1356F mutant PfPI4KIIIβ proteins without selection of the parasites on either imidazopyrazine or quinoxaline were ∼4-, 5-, and 1 (not resistant)-fold resistant to imidazopyrazine and ∼3-, 7-, and 7.5-fold resistant to quinoxaline, respectively.[10] Taken together, these previous live parasite data suggest that the Y1356F mutation of PfPI4KIIIβ does not affect the potency of imidazopyrazines but does affect the potency of the quinoxaline BQR695 and that both H1484Y and S1320L mutations modestly affect the potency for both classes.

With purified PfPI4KIIIβ now in hand, direct analysis of the effects of these mutations on drug inhibition was possible (Figure 9A). In agreement with previously published parasite growth inhibition (IC_{50}) data, we observe similar trends in relative inhibition of mutant PfPI4KIIIβ enzyme by the PI4KIIIβ-targeting drugs. While in some cases the absolute values for the fold shift in purified enzyme EC_{50} versus the fold shift in parasite IC_{50} differ, the relative effects of each mutation on drug potency versus purified PfPI4KIIIβ are consistent with those reported for live parasites. For example, as shown in Figure 9A, the S1320L mutation decreases the potency of KDU691 by >175-fold for the purified enzyme whereas a

https://dx.doi.org/10.1021/acs.biochem.0c00259
Biochemistry 2020, 59, 2494−2506

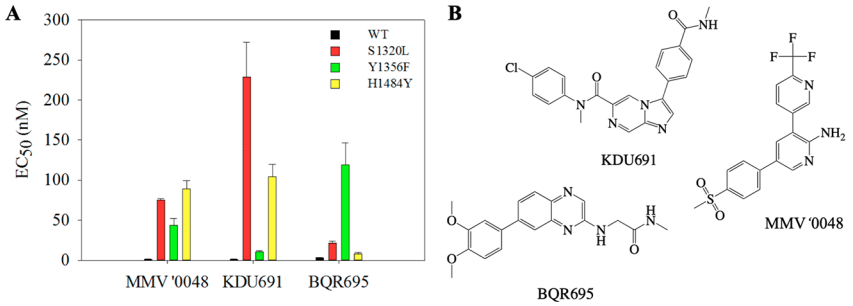

Figure 9. (A) Inhibition of purified PfPI4KIIIβ mutants by putative PI4KIIIβ-targeting drugs. (B) Chemical structures of MMV '0048, KDU691, and BQR695.

smaller (5-fold) shift in drug IC_{50} was previously measured for parasites expressing this mutant PfPI4KIIIβ.[10] H1484Y and Y1356F mutations decrease the KDU691 potency by ~80- and 8-fold versus purified enzyme, respectively (Figure 9A), and were reported to shift parasite IC_{50} values by 4- and 1-fold, respectively.[10] Because many drugs have both cytostatic (growth inhibitory, quantified by IC_{50}) and cytocidal (cell kill, quantified by LD_{50}) activities, but only cytostatic (IC_{50}) activity has been measured to date for live parasites, we suggest that testing for trends in changes in cytocidal (parasiticidal) activity for these drugs upon mutation of PfPI4KIIIβ would be worthwhile.

Previously, MMV '0048 was proposed to target PfPI4KIIIβ because two novel PfPI4KIIIβ mutations (S743T and A1319V) were revealed upon MMV '0048 selection of live parasites.[12] Residue A1319 is adjacent to S1320 within the C-terminal region of the PfPI4KIIIβ N-lobe (Figure 2A). These findings suggest MMV '0048 likely interacts with PfPI4KIIIβ differently relative to the other drugs, perhaps with the PfPI4KIIIβ N-lobe in such a way that alters the conformation of the ATP binding pocket. MMV '0048 activity versus imidazopyrazine and quinoxaline resistant mutants (S1320L, Y1356F, and H1484Y) is also shown (Figure 9A). Previously, the cross-resistance for MMV '0048 versus imidazopyrazine and BQR695 resistant strains harboring PfPI4KIIIβ mutations S1320L and H1484Y showed ~3-fold shifts in parasite IC_{50} for MMV '0048.[12] Again, although shifts in *in vivo* versus *in vitro* activity are not identical, we see a consistent pattern of potency shifts for these PfPI4KIIIβ-targeting drugs versus mutant purified enzyme and live parasites. The Y1356F mutation also appears to reduce MMV '0048 potency versus PfPI4KIIIβ (~30-fold), which is surprising if PfPI4KIIIβ is the only target of the drug because the Y1356F mutation was not previously found to appreciably affect the drug's antiparasitic cytostatic potency.[12] This residue is located in the hinge region between the N-lobe and catalytic domain and may interact with MMV '0048 near the ATP binding pocket.[23] Regardless, overall these findings confirm MMV '0048 targeting of PfPI4KIIIβ likely via contacts with the enzyme's N-lobe, suggesting an MOA unique from other kinase inhibitors, which typically act as ATP antagonists via direct binding to the active conformation of the ATP binding pocket.[61,62] Alternatively, perhaps '0048 is binding a "non-active" conformation of the enzyme or to an allosteric site. These questions and many others merit additional study.

CONCLUSIONS

Data in this paper may be summarized as follows:

1) Via direct activity measurements, we confirm that PlasmoDB# PF3D7_0509800 does indeed encode a PfPI4K "type IIIβ" enzyme as previously suggested from sequence alignments,
2) PfPI4KIIIβ shows important features that distinguish it from human PIK orthologues, which can presumably be leveraged in anti - PfPI4KIIIβ drug design,
3) Previously described imidazopyrazine and quinoxaline lead PfPI4KIIIβ inhibitors appear specific for PfPI4KIIIβ versus related PfPI3KIII (PfVps34), whereas at least one lead 2-aminopyridine inhibits both enzymes with approximately equal potency.

We suggest that a particularly useful class of next generation ACTs would include "PIKi" partner drugs that target multiple essential *P. falciparum* PIKs. In future work testing and optimizing these, we also suggest that LD_{50} vs IC_{50} measurements of drug potencies for strains harboring mutant PIKs are needed in order to better test relationships between *in vitro* enzyme potencies vs antimalarial activity.[63] Although insufficient data are currently available, it may be the case that, similar to quinoline antimalarials, these drugs both kill *P. falciparum* and inhibit parasite growth, but perhaps upon different dosages or times of exposure.[63] If so, it is presently unclear whether mutations in PfPI4KIIIβ confer resistance to the cytocidal or cytostatic effects of these drugs (or both). Such complexities may explain the conserved, but non-linear pattern of relative shifts in drug *in vitro* EC_{50} and *in vivo* IC_{50} measured for a purified enzyme vs parasites expressing the same enzyme.

Since PIP lipid abundance affects multiple intracellular pathways, parasiticidal vs cytostatic activities of PfPI4KIIIβ-specific compounds and PfVps34 inhibitors[11,16] likely affect multiple pathways, such as the autophagy-like pathway for *P. falciparum*, previously associated with resistance to the 'cidal (but not 'static) activity of chloroquine.[17] While the PfPI4KIIIβ residues found to be mutated in drug resistant parasites are likely important for drug binding, they are only a few among many residues involved in optimal drug binding and enzyme activity. Additional structural and functional studies of these kinases will further inform drug design.

Interestingly, we find >20x increases in *in vitro* S1320L and H1484Y PfPI4KIIIβ EC_{50} shifts compared to parasite IC_{50} shifts for MMV '0048 and KDU691, respectively (Figure 9A). It is not unusual to observe *in vitro* drug potencies 10-fold greater than what is observed *in vivo* due to various physical–chemical and/or physiological complications, such as drug uptake, drug or target sequestration, and target binding pocket accessibility *in vitro* vs *in vivo*. However, these differences nonetheless suggest the need for additional biochemical

https://dx.doi.org/10.1021/acs.biochem.0c00259
Biochemistry 2020, 59, 2494−2506

analyses of drug-target interactions to better inform future drug design. The H1484Y mutation was originally found in an imidazopyrazine-resistant parasite clone that had been pressured with the KDU691-like imidazopyrazine compound KAI407,[10] so the >175-fold shift in KDU691 EC_{50} vs H1484Y PfPI4KIIIβ clearly highlights the importance of this residue in imidazopyrazine binding to N-CAT PfPI4KIIIβ. Because S1320 is adjacent to the mutant residue selected in some MMV '0048-resistant parasites (A1319V), the elevated fold-shift in MMV '0048 EC_{50} vs S1320L PfPI4KIIIβ could be attributed to a similar phenomenon. Similarly, the shift in BQR695 EC_{50} vs Y1356F PfPI4KIIIβ compared to the shift observed in drug IC_{50} for parasites expressing the enzyme is likely emphasizing the essentiality of this residue for BQR695 binding.

Previously, the crystal structure of BQR695-bound HsPI4-KIIIβ suggested ATP binding pocket residue *Hs*-L383 (corresponding to *Pf*-L836) may at least partially assist BQR695 hydrogen bonding with *Hs*-V598 (corresponding to *Pf*-V1357) and might therefore be important for the drug's selectivity versus PI4KIIIβ.[54] *Pf*-L836 is located within the N-terminal region of the N-lobe, which is not present in our expressed PfPI4KIIIβ N-CAT protein. The lack of this residue in the N-CAT protein perhaps increases the importance of the Y1356 and V1357 hinge region residues for BQR695 binding, thereby resulting in a larger reduction of BQR695 potency versus the mutant Y1356F PfPI4KIIIβ N-CAT enzyme as reported here. Because the crystal structure of PfPI4KIIIβ has not yet been determined, a more detailed understanding of the relative importance of additional N-terminal residues for drug binding is limited. Further studies with additional enzyme constructs should resolve these issues.

Further work with *P. vivax* PI4KIIIβ might also help answer the remaining questions. We note that although they are similar, the activities of *P. falciparum* and *P. vivax* PI4KIIIβ enzymes do not appear to be identical. In particular, inhibition by PI4K-targeting drugs shows different potencies. The *Pf* and *Pv* PI4KIIIβ enzymes are 58.3% homologous overall, which increases to 97% for the 313 C-terminal catalytic site residues. Nonconserved residues in the catalytic domain or the adjacent N-lobe and hinge regions are likely responsible for differences in drug potency versus the two enzymes, whether by loss of key binding contacts or alterations in binding pocket size and conformation. It will prove useful to explore these differences, as well as those revealed by careful comparison between *Hs* and *Pf* orthologues. As discussed previously, two novel PfPI4KIIIβ mutations (S743T and A1319V) were recently revealed upon MMV '0048 selection of live parasites.[12] Testing inhibition of these mutant enzymes by other lead PIKi should prove to be interesting.[11]

With a few exceptions, relatively few studies have explored PfPIKs.[64] Of six that can be identified within the genome, to date only three have been studied in depth, and only two have been purified (ref 16 and this paper). However, candidate drug lead compounds targeting these enzymes are very attractive candidates for next-generation ACT partner drugs. To develop these drugs further, it is essential that they be tested versus purified enzymes. In part, this is because extensive prior experience with targeting eukaryotic PIKs[20,65] has shown that some compounds may inhibit multiple PIK isoforms, as we now also find to be the case for one attractive lead PfPIKi (MMV '0048). Information related to single versus dual kinase potency is important for the design of future antimalarial drug therapies.

■ ASSOCIATED CONTENT

Accession Codes

PfVps34, Uniprot Q8I3V5; PfPI4KIIIβ, Uniprot Q8I406; PvPI4KIIIβ, Uniprot A5KB26; HsPI4KB, Uniprot Q9UBF8; ScPIK1, Uniprot P39104; HsVps34, Uniprot Q8NEB9; ScVps34, Uniprot P22543.

■ AUTHOR INFORMATION

Corresponding Author

Paul D. Roepe − *Department of Chemistry and Department of Biochemistry and Cellular and Molecular Biology, Georgetown University, Washington, D.C. 20057, United States;* orcid.org/0000-0002-7079-3793; Phone: 202-687-7300; Email: roepep@georgetown.edu

Author

Anna R. Sternberg − *Department of Chemistry and Department of Biochemistry and Cellular and Molecular Biology, Georgetown University, Washington, D.C. 20057, United States;* orcid.org/0000-0003-1564-7870

Complete contact information is available at: https://pubs.acs.org/10.1021/acs.biochem.0c00259

Funding

Supported by the National Institutes of Health (RO1 AII111962 to P.D.R.).

Notes

The authors declare no competing financial interest.

■ ACKNOWLEDGMENTS

The authors thank our laboratory colleagues Dr. Matthew Hassett, Dr. Laura Heller, Dr. Kalpana Iyengar, and Mr. Bryce Riegel for technical help and advice and Dr. Tamas Balla (Section on Molecular Signal Transduction, National Institutes of Health) for helpful conversations.

■ ABBREVIATIONS

ACT, artemisinin combination therapy; ART, artemisinin; ATM, artemether; ATS, artesunate; B-PI4P, biotinylated phosphatidylinositol 4-phosphate; CAT, catalytic domain; CQ, chloroquine; DCP, delayed clearance phenotype; DHA, dihydroartemisinin; EC_{50}, drug concentration that inhibits 50% of purified enzyme activity; ELISA, enzyme-linked immunosorbent assay; HsVps34, *H. sapiens* vacuolar protein sorting 34 protein; IC_{50}, drug concentration that inhibits 50% of parasite growth in culture; LD_{50}, drug concentration that kills 50% of parasites in culture; LF, lumefantrine; MMV '0048, MMV3900048; MOA, mechanism of action; MQ, mefloquine; PfPI3K, *P. falciparum* phosphatidylinositol 3-kinase; PfPI3KIII, *P. falciparum* phosphatidylinositol 3-kinase class III; PfPI4K, *P. falciparum* phosphatidylinositol 4-kinase; PfPI4KIIIβ, *P. falciparum* phosphatidylinositol 4-kinase type IIIβ protein (gene in italics); PfPIK, *P. falciparum* phosphatidylinositol kinase; PfPIKi, *P. falciparum* phosphatidylinositol kinase inhibitor; PfVps34, *P. falciparum* vacuolar protein sorting 34 protein (gene in italics); PI, phosphatidylinositol; PI3K, phosphatidylinositol 3-kinase; PI3P, phosphatidylinositol 3-phosphate; PI4K, phosphatidylinositol 4-kinase; PI4KB, human phosphatidylinositol 4-kinase type IIIβ protein;

https://dx.doi.org/10.1021/acs.biochem.0c00259
Biochemistry 2020, 59, 2494−2506

PI4KIIIβ, phosphatidylinositol 4-kinase type IIIβ; PI4P, phosphatidylinositol 4-phosphate; PIK, phosphatidylinositol kinase; PIKi, phosphatidylinositol kinase inhibitor; PIP, phosphatidylinositol phosphate; PIP4K2C, phosphatidylinositol-5-phosphate 4-kinase type IIγ; PPQ, piperaquine; PvPI4KIIIβ, *P. vivax* phosphatidylinositol 4-kinase type IIIβ; RSA, ring stage assay; SNP, single-nucleotide polymorphism; SP, sulfadoxine/pyrimethamine.

REFERENCES

(1) Noedl, H., Socheat, D., and Satimai, W. (2009) Artemisinin-resistant malaria in Asia. *N. Engl. J. Med. 361*, 540−541.

(2) van der Pluijm, R. W., Imwong, M., Chau, N. H., Hoa, N. T., Thuy-Nhien, N. T., Thanh, N. V., Jittamala, P., Hanboonkunupakarn, B., Chutasmit, K., Saelow, C., Runjarern, R., Kaewmok, W., Tripura, R., Peto, T. J., Yok, S., Suon, S., Sreng, S., Mao, S., Oun, S., Yen, S., Amaratunga, C., Lek, D., Huy, R., Dhorda, M., Chotivanich, K., Ashley, E. A., Mukaka, M., Waithira, N., Cheah, P. Y., Maude, R. J., Amato, R., Pearson, R. D., Gonçalves, S., Jacob, C. G., Hamilton, W. L., Fairhurst, R. M., Tarning, J., Winterberg, M., Kwiatkowski, D. P., Pukrittayakamee, S., Hien, T. T., Day, N. P., Miotto, O., White, N. J., and Dondorp, A. M. (2019) Determinants of dihydroartemisinin-piperaquine treatment failure in Plasmodium falciparum malaria in Cambodia, Thailand, and Vietnam: a prospective clinical, pharmacological, and genetic study. *Lancet Infect. Dis. 19*, 952.

(3) Hamilton, W. L., Amato, R., van der Pluijm, R. W., Jacob, C. G., Quang, H. H., Thuy-Nhien, N. T., Hien, T. T., Hongvanthong, B., Chindavongsa, K., Mayxay, M., Huy, R., Leang, R., Huch, C., Dysoley, L., Amaratunga, C., Suon, S., Fairhurst, R. M., Tripura, R., Peto, T. J., Sovann, Y., Jittamala, P., Hanboonkunupakarn, B., Pukrittayakamee, S., Chau, N. H., Imwong, M., Dhorda, M., Vongpromek, R., Chan, X. H. S., Maude, R. J., Pearson, R. D., Nguyen, T., Rockett, K., Drury, E., Gonçalves, S., White, N. J., Day, N. P., Kwiatkowski, D. P., Dondorp, A. M., and Miotto, O. (2019) Evolution and expansion of multidrug-resistant malaria in southeast Asia: a genomic epidemiology study. *Lancet Infect. Dis. 19*, 943.

(4) Noedl, H., Se, Y., Schaecher, K., Smith, B. L., Socheat, D., and Fukuda, M. M. (2008) Evidence of artemisinin-resistant malaria in western Cambodia. *N. Engl. J. Med. 359*, 2619−2620.

(5) Dondorp, A. M., Nosten, F., Yi, P., Das, D., Phyo, A. P., Tarning, J., Lwin, K. M., Ariey, F., Hanpithakpong, W., Lee, S. J., Ringwald, P., Silamut, K., Imwong, M., Chotivanich, K., Lim, P., Herdman, T., An, S. S., Yeung, S., Singhasivanon, P., Day, N. P., Lindegardh, N., Socheat, D., and White, N. J. (2009) Artemisinin resistance in Plasmodium falciparum malaria. *N. Engl. J. Med. 361*, 455−467.

(6) Amaratunga, C., Sreng, S., Suon, S., Phelps, E. S., Stepniewska, K., Lim, P., Zhou, C., Mao, S., Anderson, J. M., Lindegardh, N., Jiang, H., Song, J., Su, X. Z., White, N. J., Dondorp, A. M., Anderson, T. J., Fay, M. P., Mu, J., Duong, S., and Fairhurst, R. M. (2012) Artemisinin-resistant Plasmodium falciparum in Pursat province, western Cambodia: a parasite clearance rate study. *Lancet Infect. Dis. 12*, 851−858.

(7) Witkowski, B., Amaratunga, C., Khim, N., Sreng, S., Chim, P., Kim, S., Lim, P., Mao, S., Sopha, C., Sam, B., Anderson, J. M., Duong, S., Chuor, C. M., Taylor, W. R., Suon, S., Mercereau- Puijalon, O., Fairhurst, R. M., and Menard, D. (2013) Novel phenotypic assays for the detection of artemisinin-resistant Plasmodium falciparum malaria in Cambodia: in-vitro and ex-vivo drug- response studies. *Lancet Infect. Dis. 13*, 1043−1049.

(8) Plouffe, D., Brinker, A., McNamara, C., Henson, K., Kato, N., Kuhen, K., Nagle, A., Adrián, F., Matzen, J. T., Anderson, P., Nam, T. G., Gray, N. S., Chatterjee, A., Janes, J., Yan, S. F., Trager, R., Caldwell, J. S., Schultz, P. G., Zhou, Y., and Winzeler, E. A. (2008) In silico activity profiling reveals the mechanism of action of antimalarials discovered in a high-throughput screen. *Proc. Natl. Acad. Sci. U. S. A. 105*, 9059−9064.

(9) Younis, Y., Douelle, F., Feng, T. S., González Cabrera, D., Le Manach, C., Nchinda, A. T., Duffy, S., White, K. L., Shackleford, D. M., Morizzi, J., Mannila, J., Katneni, K., Bhamidipati, R., Zabiulla, K. M., Joseph, J. T., Bashyam, S., Waterson, D., Witty, M. J., Hardick, D., Wittlin, S., Avery, V., Charman, S. A., and Chibale, K. (2012) 3,5-Diaryl-2-aminopyridines as a novel class of orally active antimalarials demonstrating single dose cure in mice and clinical candidate potential. *J. Med. Chem. 55*, 3479−3487.

(10) McNamara, C. W., Lee, M. C., Lim, C. S., Lim, S. H., Roland, J., Simon, O., Yeung, B. K., Chatterjee, A. K., McCormack, S. L., Manary, M. J., Zeeman, A. M., Dechering, K. J., Kumar, T. S., Henrich, P. P., Gagaring, K., Ibanez, M., Kato, N., Kuhen, K. L., Fischli, C., Nagle, A., Rottmann, M., Plouffe, D. M., Bursulaya, B., Meister, S., Rameh, L., Trappe, J., Haasen, D., Timmerman, M., Sauerwein, R. W., Suwanarusk, R., Russell, B., Renia, L., Nosten, F., Tully, D. C., Kocken, C. H., Glynne, R. J., Bodenreider, C., Fidock, D. A., Diagana, T. T., and Winzeler, E. A. (2013) Targeting Plasmodium PI(4)K to eliminate malaria. *Nature 504*, 248−253.

(11) Mott, B. T., Eastman, R. T., Guha, R., Sherlach, K. S., Siriwardana, A., Shinn, P., McKnight, C., Michael, S., Lacerda-Queiroz, N., Patel, P. R., Khine, P., Sun, H., Kasbekar, M., Aghdam, N., Fontaine, S. D., Liu, D., Mierzwa, T., Mathews-Griner, L. A., Ferrer, M., Renslo, A. R., Inglese, J., Yuan, J., Roepe, P. D., Su, X. Z., and Thomas, C. J. (2015) High-throughput matrix screening identifies synergistic and antagonistic antimalarial drug combinations. *Sci. Rep. 5*, 13891.

(12) Paquet, T., Le Manach, C., Cabrera, D. G., Younis, Y., Henrich, P. P., Abraham, T. S., Lee, M. C. S., Basak, R., Ghidelli-Disse, S., Lafuente-Monasterio, M. J., Bantscheff, M., Ruecker, A., Blagborough, A. M., Zakutansky, S. E., Zeeman, A. M., White, K. L., Shackleford, D. M., Mannila, J., Morizzi, J., Scheurer, C., Angulo-Barturen, I., Martínez, M. S., Ferrer, S., Sanz, L. M., Gamo, F. J., Reader, J., Botha, M., Dechering, K. J., Sauerwein, R. W., Tungtaeng, A., Vanachayangkul, P., Lim, C. S., Burrows, J., Witty, M. J., Marsh, K. C., Bodenreider, C., Rochford, R., Solapure, S. M., Jiménez-Díaz, M. B., Wittlin, S., Charman, S. A., Donini, C., Campo, B., Birkholtz, L. M., Hanson, K. K., Drewes, G., Kocken, C. H. M., Delves, M. J., Leroy, D., Fidock, D. A., Waterson, D., Street, L. J., and Chibale, K. (2017) Antimalarial efficacy of MMV390048, an inhibitor of Plasmodium phosphatidylinositol 4-kinase. *Sci. Transl. Med. 9*, eaad9735.

(13) PF3D7_0509800 phosphatidylinositol 4-kinase: Transcriptomics; PlasmoDB, 2019. https://plasmodb.org/plasmo/app/record/gene/PF3D7_0509800#category:transcriptomics (accessed 2019-04-29).

(14) Bushell, E., Gomes, A. R., Sanderson, T., Anar, B., Girling, G., Herd, C., Metcalf, T., Modrzynska, K., Schwach, F., Martin, R. E., Mather, M. W., McFadden, G. I., Parts, L., Rutledge, G. G., Vaidya, A. B., Wengelnik, K., Rayner, J. C., and Billker, O. (2017) Functional Profiling of a Plasmodium Genome Reveals an Abundance of Essential Genes. *Cell 170*, 260−272.

(15) Tawk, L., Chicanne, G., Dubremetz, J. F., Richard, V., Payrastre, B., Vial, H. J., Roy, C., and Wengelnik, K. (2010) Phosphatidylinositol 3-phosphate, an essential lipid in Plasmodium, localizes to the food vacuole membrane and the apicoplast. *Eukaryotic Cell 9*, 1519−1530.

(16) Hassett, M. R., Sternberg, A. R., Riegel, B. E., Thomas, C. J., and Roepe, P. D. (2017) Heterologous Expression, Purification, and Functional Analysis of Plasmodium falciparum Phosphatidylinositol 3′-Kinase. *Biochemistry 56*, 4335−4345.

(17) Gaviria, D., Paguio, M. F., Turnbull, L. B., Tan, A., Siriwardana, A., Ghosh, D., Ferdig, M. T., Sinai, A. P., and Roepe, P. D. (2013) A process similar to autophagy is associated with cytocidal chloroquine resistance in Plasmodium falciparum. *PLoS One 8*, e79059.

(18) Zhang, H., Howard, E. M., and Roepe, P. D. (2002) Analysis of the antimalarial drug resistance protein Pfcrt expressed in yeast. *J. Biol. Chem. 277*, 49767−49775.

(19) Amoah, L. E., Lekostaj, J. K., and Roepe, P. D. (2007) Heterologous expression and ATPase activity of mutant versus wild type PfMDR1 protein. *Biochemistry 46*, 6060−6073.

(20) Hassett, M. R., Sternberg, A. R., and Roepe, P. D. (2017) Inhibition of Human Class I vs Class III Phosphatidylinositol 3′-Kinases. *Biochemistry 56*, 4326−4334.

https://dx.doi.org/10.1021/acs.biochem.0c00259
Biochemistry 2020, 59, 2494−2506

(21) Baro, N. K., Pooput, C., and Roepe, P. D. (2011) Analysis of chloroquine resistance transporter (CRT) isoforms and orthologues in S. cerevisiae yeast. *Biochemistry 50*, 6701−6710.
(22) Yachdav, G., Kloppmann, E., Kajan, L., Hecht, M., Goldberg, T., Hamp, T., Honigschmid, P., Schafferhans, A., Roos, M., Bernhofer, M., Richter, L., Ashkenazy, H., Punta, M., Schlessinger, A., Bromberg, Y., Schneider, R., Vriend, G., Sander, C., Ben-Tal, N., and Rost, B. (2014) PredictProtein − an open resource for online prediction of protein structural and functional features. *Nucleic Acids Res. 42*, W337−W343.
(23) Burke, J. E., Inglis, A. J., Perisic, O., Masson, G. R., McLaughlin, S. H., Rutaganira, F., Shokat, K. M., and Williams, R. L. (2014) Structures of PI4KIIIβ complexes show simultaneous recruitment of Rab11 and its effectors. *Science 344*, 1035−1038.
(24) Kruger, T., Sanchez, C. P., and Lanzer, M. (2010) Complementation of *Saccharomyces cerevisiae pik1*^{ts} by a phosphatidylinositol 4-kinase from *Plasmodium falciparum*. *Mol. Biochem. Parasitol. 172*, 149−151.
(25) Flanagan, C. A., Schnieders, E. A., Emerick, A. W., Kunisawa, R., Admon, A., and Thorner, J. (1993) Phosphatidylinositol 4-kinase: gene structure and requirement for yeast cell viability. *Science 262*, 1444−1448.
(26) Nakagawa, T., Goto, K., and Kondo, H. (1996) Cloning and characterization of a 92 kDa soluble phosphatidylinositol 4-kinase. *Biochem. J. 320*, 643−649.
(27) Meyers, R., and Cantley, L. C. (1997) Cloning and characterization of a wortmannin-sensitive human phosphatidylinositol 4-kinase. *J. Biol. Chem. 272*, 4384−4390.
(28) Gehrmann, T., and Heilmeyer, L. M., Jr. (1998) Phosphatidylinositol 4-kinases. *Eur. J. Biochem. 253*, 357−370.
(29) Altan-Bonnet, N., and Balla, T. (2012) Phosphatidylinositol 4-kinases: hostages harnessed to build panviral replication platforms. *Trends Biochem. Sci. 37*, 293−302.
(30) Boura, E., and Nencka, R. (2015) Phosphatidylinositol 4-kinases: Function, structure, and inhibition. *Exp. Cell Res. 337*, 136−145.
(31) Waterhouse, A., Bertoni, M., Bienert, S., Studer, G., Tauriello, G., Gumienny, R., Heer, F. T., de Beer, T. A. P., Rempfer, C., Bordoli, L., Lepore, R., and Schwede, T. (2018) SWISS-MODEL: homology modelling of protein structures and complexes. *Nucleic Acids Res. 46*, W296−W303.
(32) LaCount, D. J., Vignali, M., Chettier, R., Phansalkar, A., Bell, R., Hesselberth, J. R., Schoenfeld, L. W., Ota, I., Sahasrabudhe, S., Kurschner, C., Fields, S., and Hughes, R. E. (2005) A protein interaction network of the malaria parasite Plasmodium falciparum. *Nature 438*, 103−107.
(33) Miller, S., Tavshanjian, B., Oleksy, A., Perisic, O., Houseman, B. T., Shokat, K. M., and Williams, R. L. (2010) Shaping development of autophagy inhibitors with the structure of the lipid kinase Vps34. *Science 327*, 1638−1642.
(34) Leondaritis, G., Siokos, J., Skaripa, I., and Galanopoulou, D. (2013) Genome-Wide Analysis of the Phosphoinositide Kinome from Two Ciliates Reveals Novel Evolutionary Links for Phosphoinositide Kinases in Eukaryotic Cells. *PLoS One 8*, e78848.
(35) Walker, E. H., Perisic, O., Ried, C., Stephens, L., and Williams, R. L. (1999) Structural insights into phosphoinositide 3-kinase catalysis and signaling. *Nature 402*, 313−320.
(36) Balla, A., Tuymetova, G., Barshishat, M., Geiszt, M., and Balla, T. (2002) Characterization of Type II Phosphatidylinositol 4-Kinase Isoforms Reveals Association of the Enzymes with Endosomal Vesicular Compartments. *J. Biol. Chem. 277*, 20041−20050.
(37) Endemann, G., Dunn, S. N., and Cantley, L. C. (1987) Bovine brain contains two types of phosphatidylinositol kinase. *Biochemistry 26*, 6845−6852.
(38) Balla, A., and Balla, T. (2006) Phosphatidylinositol 4-kinases: old enzymes with emerging functions. *Trends Cell Biol. 16*, 351−361.
(39) Morgan, S. J., Smith, A. D., and Parker, P. J. (1990) Purification and characterization of bovine brain type I phosphatidylinositol kinase. *Eur. J. Biochem. 191*, 761−767.
(40) Stephens, L., Cooke, F. T., Walters, R., Jackson, T., Volinia, S., Gout, I., Waterfield, M. D., and Hawkins, P. T. (1994) Characterization of a phosphatidylinositol-specific phosphoinositide 3-kinase from mammalian cells. *Curr. Biol. 4*, 203−214.
(41) PI4-Kinase II α (PI4KIIa), active; Image [Online], Echelon Biosciences, Salt Lake City, UT (accessed 2019-05-12) (https://www.echelon-inc.com/content/EBI/product/images/1648.gif).
(42) PI4-Kinase II β (PI4KIIb), active; Image [Online], Echelon Biosciences, Salt Lake City, UT (accessed 2019-05-12) (https://www.echelon-inc.com/content/EBI/product/images/1647.gif).
(43) PI4K2B, active, GST tagged, human; Datasheet [Online] (2011) Sigma-Aldrich, St. Louis, MO (https://www.sigmaaldrich.com/content/dam/sigma-aldrich/docs/Sigma/Datasheet/9/srp5064dat.pdf).
(44) Wetzker, R., Klinger, R., Hsuan, J., Fry, M. J., Kauffmann-Zeh, A., Müller, E., Frunder, H., and Waterfield, M. (1991) Purification and characterization of phosphatidylinositol 4-kinase from human erythrocyte membranes. *Eur. J. Biochem. 200*, 179−185.
(45) Porter, F. D., Li, Y. S., and Deuel, T. F. (1988) Purification and characterization of a phosphatidylinositol 4-kinase from bovine uteri. *J. Biol. Chem. 263*, 8989−8995.
(46) Downing, G. J., Kim, S., Nakanishi, S., Catt, K. J., and Balla, T. (1996) Characterization of a soluble adrenal phosphatidylinositol 4-kinase reveals wortmannin sensitivity of type III phosphatidylinositol kinases. *Biochemistry 35*, 3587−3594.
(47) PI4KA, Active; Datasheet [Online] (2019) SignalChem, Richmond, BC (https://www.signalchem.com/shared_product_sheets/L2026-9.pdf).
(48) PI4KB, Active, GST tagged, human; Datasheet [Online] (2011) Sigma-Aldrich, St. Louis, MO (https://www.sigmaaldrich.com/content/dam/sigma-aldrich/docs/Sigma/Datasheet/9/srp5065dat.pdf).
(49) PI4KB, Active; Datasheet [Online] (2016) SignalChem, Richmond, BC (https://www.signalchem.com/shared_product_sheets/N066-3.pdf).
(50) PI4-Kinase β (PI4Kb), active; Image [Online], Echelon Biosciences, Salt Lake City, UT (accessed 2019-04-28) (https://www.echelon-inc.com/content/EBI/product/images/1649.gif).
(51) ADP-Glo Lipid Kinase Systems; Technical Manual [Online] (2015) Promega Corp., Madison, WI (https://www.promega.com/-/media/files/resources/protocols/technical-manuals/101/adp-glo-lipid-kinase-assay-protocol.pdf).
(52) Tai, A. W., Bojjireddy, N., and Balla, T. (2011) A homogeneous and nonisotopic assay for phosphatidylinositol 4-kinases. *Anal. Biochem. 417*, 97−102.
(53) Garcia-Bustos, J. F., Marini, F., Stevenson, I., Frei, C., and Hall, M. N. (1994) PIK1, an essential phosphatidylinositol 4-kinase associated with the yeast nucleus. *EMBO J. 13*, 2352−2361.
(54) Fowler, M. L., McPhail, J. A., Jenkins, M. L., Masson, G. R., Rutaganira, F. U., Shokat, K. M., Williams, R. L., and Burke, J. E. (2016) Using hydrogen deuterium exchange mass spectrometry to engineer optimized constructs for crystallization of protein complexes: Case study of PI4KIIIβ with Rab11. *Protein Sci. 25*, 826−839.
(55) Kandepedu, N., Gonzàlez Cabrera, D., Eedubilli, S., Taylor, D., Brunschwig, C., Gibhard, L., Njoroge, M., Lawrence, N., Paquet, T., Eyermann, C. J., Spangenberg, T., Basarab, G. S., Street, L. J., and Chibale, K. (2018) Identification, Characterization, and Optimization of 2,8-Disubstituted-1,5-naphthyridines as Novel Plasmodium falciparum Phosphatidylinositol-4-kinase Inhibitors with in Vivo Efficacy in a Humanized Mouse Model of Malaria. *J. Med. Chem. 61*, 5692−5703.
(56) Brunschwig, C., Lawrence, N., Taylor, D., Abay, E., Njoroge, M., Basarab, G. S., Le Manach, C., Paquet, T., Gonzàlez Cabrera, D., Nchinda, A. T., de Kock, C., Wiesner, L., Denti, P., Waterson, D., Blasco, B., Leroy, D., Witty, M. J., Donini, C., Duffy, J., Wittlin, S., White, K. L., Charman, S. A., Jiménez-Díaz, M. B., Angulo-Barturen, I., Herreros, E., Gamo, F. J., Rochford, R., Mancama, D., Coetzer, T. L., van der Watt, M. E., Reader, J., Birkholtz, L. M., Marsh, K. C., Solapure, S. M., Burke, J. E., McPhail, J. A., Vanaerschot, M., Fidock,

https://dx.doi.org/10.1021/acs.biochem.0c00259
Biochemistry 2020, 59, 2494−2506

D. A., Fish, P. V., Siegl, P., Smith, D. A., Wirjanata, G., Noviyanti, R., Price, R. N., Marfurt, J., Silue, K. D., Street, L. J., and Chibale, K. (2018) UCT943, a Next-Generation Plasmodium falciparum PI4K Inhibitor Preclinical Candidate for the Treatment of Malaria. *Antimicrob. Agents Chemother. 62*, e00012−18.

(57) Ibrahim, M. A. A., Abdelrahman, A. H. M., and Hassan, A. M. A. (2019) Identification of novel Plasmodium falciparum PI4KB inhibitors as potential anti-malarial drugs: Homology modeling, molecular docking and molecular dynamics simulations. *Comput. Biol. Chem. 80*, 79−89.

(58) Hassett, M. R. (2017) Studies of Malarial Parasite Chloroquine Resistance Transporter and Kinase Proteins: Key Targets for Evolving Drug Therapies. Ph.D. Dissertation, Georgetown University, Washington, DC.

(59) Liu, Q., Wang, J., Kang, S. A., Thoreen, C. C., Hur, W., Ahmed, T., Sabatini, D. M., and Gray, N. S. (2011) Discovery of 9-(6-aminopyridin-3-yl)-1-(3-(trifluoromethyl)phenyl)benzo[h][1,6]-naphthyridin-2(1H)-one (Torin2) as a potent, selective, and orally available mammalian target of rapamycin (mTOR) inhibitor for treatment of cancer. *J. Med. Chem. 54*, 1473−1480.

(60) Markman, B., Tabernero, J., Krop, I., Shapiro, G. I., Siu, L., Chen, L. C., Mita, M., Melendez Cuero, M., Stutvoet, S., Birle, D., Anak, O., Hackl, W., and Baselga, J. (2012) Phase I safety, pharmacokinetic, and pharmacodynamic study of the oral phosphatidylinositol-3-kinase and mTOR inhibitor BGT226 in patients with advanced solid tumors. *Ann. Oncol 23*, 2399−2408.

(61) Zhang, J., Yang, P. L., and Gray, N. S. (2009) Targeting cancer with small molecule kinase inhibitors. *Nat. Rev. Cancer 9*, 28−39.

(62) Bhullar, K. S., Lagaron, N. O., McGowan, E. M., Parmar, I., Jha, A., Hubbard, B. P., and Rupasinghe, H. P. V. (2018) Kinase-targeted cancer therapies: progress, challenges and future directions. *Mol. Cancer 17*, 48−67.

(63) Roepe, P. D. (2014) To kill or not to kill, that is the question: cytocidal antimalarial drug resistance. *Trends Parasitol. 30*, 130−135.

(64) Hassett, M. R., and Roepe, P. D. (2018) PIK-ing New Malaria Chemotherapy. *Trends Parasitol. 34*, 925−927.

(65) Mayer, I. A., and Arteaga, C. L. (2016) The PI3K/AKT Pathway as a Target for Cancer Treatment. *Annu. Rev. Med. 67*, 11−28.

https://dx.doi.org/10.1021/acs.biochem.0c00259
Biochemistry 2020, 59, 2494−2506